applied sciences

MDPI

Article

Quantitative Investigation of Surface Charge Distribution and Point Probing Characteristics of Spherical Scattering Electrical Field Probe for Precision Measurement of Miniature Internal Structures with High Aspect Ratios

Xingyuan Bian [1,2], Junning Cui [1,2,*], Yesheng Lu [1,2], Yamin Zhao [1,2], Zhongyi Cheng [1,2] and Jiubin Tan [1,2]

[1] Center of Ultra-Precision Optoelectronic Instrument Engineering, Harbin Institute of Technology, Harbin 150080, China; bianxingyuan@hit.edu.cn (X.B.); 13B901016@hit.edu.cn (Y.L.); zhaoyamin@163.com (Y.Z.); 19B901007@stu.hit.edu.cn (Z.C.); jbtan@hit.edu.cn (J.T.)

[2] Key Lab of Ultra-Precision Intelligent Instrumentation (Harbin Institute of Technology), Ministry of Industry and Information Technology, Harbin 150080, China

* Correspondence: cuijunning@126.com or cuijunning@hit.edu.cn

Received: 21 June 2020; Accepted: 28 July 2020; Published: 30 July 2020

check for updates

Abstract: For precision measurement of miniature internal structures with high aspect ratios, a spherical scattering electrical field probe (SSEP) is proposed based on charge signal detection. The characteristics and laws governing surface charge distribution on the probing ball of the SSEP are analyzed, with the spherical scattering electrical field modeled using a 3D seven-point finite difference method. The model is validated with finite element simulation by comparing with the analysis results of typical situations, in which probing balls of different diameters are used to probe a grounded plane with a probing gap of 0.3 μm. Results obtained with the proposed model and finite element method (FEM) simulation indicate that 31% of the total surface charge on a ϕ1 mm probing ball concentrates in an area that occupies 1% of the total probing ball surface. Moreover, this surface charge concentration remains unchanged when the surface being measured varies in geometry, or when the probing gap varies in sensing range. Based on this, the SSEP has realized approximate point probing capability with a virtual "needle" of electrical effect. Together with its non-contact sensing characteristics and 3D isotropy, it can, therefore, be concluded that the SSEP has great potential to be an ideal solution for precision measurement of miniature internal structures with high aspect ratios.

Keywords: surface charge distribution; point probing characteristics; spherical scattering electrical field probe; miniature internal structures; high aspect ratios

1. Introduction

Nowadays, parts adopting miniature internal structures with high aspect ratios, such as deep, small holes and grooves [1,2], can transmit working medium, energy, and information over relatively long distances, and are of great significance in achieving high integration and low energy consumption in the aviation, aerospace, and automotive industries. The machining precision of these structures often reaches the sub-micron level; moreover, their aspect ratio is up to several tens and even several hundreds [3–5], posing a great challenge to conventional measurement methods in terms of measurability. Various probing methods have been investigated to measure this particular kind of structure, such as miniaturized ball probes with flexible hinges [6–8], fiber optical probes [9–13], as well as other creative probing methods based on the principle of the tunneling effect [14], optical interference [15,16], pneumatics [17], capacitance [18], atomic force microscope [19], and the piezoelectric effect [20]. However, not having the three features of point probing capability, non-contact probing, and 3D isotropic sensing at the same time makes it difficult to accurately measure high aspect ratio structures with these conventional methods. As part of our efforts to find a possible solution including all of these required capabilities, a spherical scattering electrical field probe (SSEP) was proposed, based on the detection of charge signal on the probing ball, and nanometer resolution displacement sensing, non-contact probing and 3D isotropy sensing capability were achieved simultaneously [1,2]. The only unclear part of the SSEP is point probing capability, on which only qualitative analysis was performed for the time being.

The point probing capability of the SSEP is closely related to surface charge distribution on the probing ball. To analyze the point probing characteristics of the SSEP, a quantitative investigation of the spherical scattering electrical field needs to be conducted to illustrate the law of surface charge distribution. The difficulties are: (1) Conventional theoretical analysis methods [21,22] cannot complete the modeling task with complicated boundary conditions, such as the possibility that the surface being probed could be a plane, spherical, cylindrical, or free geometrical shape; (2) On the other hand, the spherical scattering electrical field is also difficult to model with conventional numerical methods due to the problem of balancing modeling accuracy and computational load. This is because the diameter of the probing ball is on a hundreds of microns to millimeter level, while the probing gap is on a micro and sub-micrometer level, and this creates a multi-scale problem, posing a challenge to gridding and computational accuracy; (3) Experimental methods [23–27] are not applicable here due to the lack of micro-/nano probes with the ability to detect the spherical scattering electrical field in the micro probing gap without introducing violent disturbance into the field. Therefore, an appropriate method of modeling and quantitative analysis of spherical scattering electrical field is the key issue to be solved for the analysis of the surface charge distribution characteristics as well as point probing characteristics of the SSEP.

In this paper, this problem is solved using a proposed 3D seven-point finite difference scheme. In the accordingly built spherical coordinates, the spherical scattering electrical field is modeled by 3D gridding and finite difference computation, solved through iteration calculation, and validated by finite element method (FEM) numerical simulation under special boundary conditions. In this way, the surface charge distribution characteristics and the resulting approximate point probing characteristics of the SSEP are quantificationally analyzed and represented.

2. Principle of SSEP

As shown in Figure 1, when an electrically conductive part is being probed, the surface being probed is grounded while the electric potential of probing ball is set to be a constant such as 1 V, and then a spherical scattering electrical field is formed. As the gap between the probing ball and the surface decreases, the surface charge on the probing ball tends to concentrate in quite a small area around the probing point, which is the closest point on the spherical surface to the surface being probed. The concentration of surface charge on the probing ball becomes obvious when the probing gap δ decreases to a certain level, which is often below the micrometer level. The spherical scattering electrical field and resulting surface charge distribution change drastically when probing gap δ changes, so high-resolution displacement sensing can be achieved by charge signal detection. The SSEP features non-contact, 3D isotropic, and approximate point probing characteristics, and can be fitted in a micro/nano-coordinate measurement machine or an analogous instrument to measure the 3D dimensions and geometry of miniature internal structures with high aspect ratios [2]. This paper focuses on the quantitative investigation of the surface charge distribution characteristics on the probing ball as well as the resulting approximate point probing capacity of the SSEP.

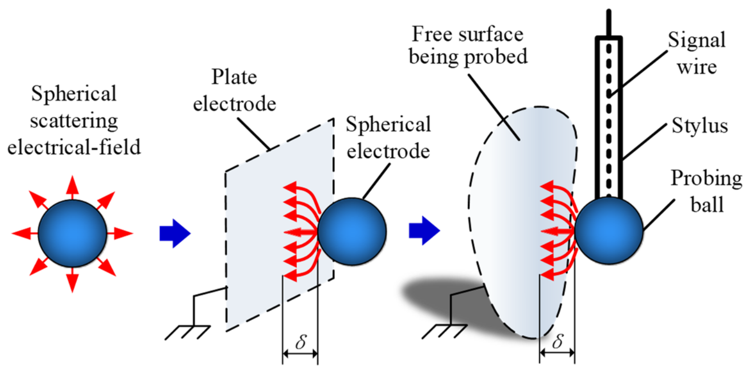

Figure 1. Working principle of spherical scattering electrical field probe (SSEP).

3. Surface Charge Distribution Modeling

Surface charge distribution modeling of the SSEP begins with spherical scattering electrical field analysis. The model of the electrical field is simplified, as shown in Figure 2. The shaft is not shown in Figure 2 because of its negligible effect, due to its delicately designed multi-coaxial-layer active shielding and grounding structure.

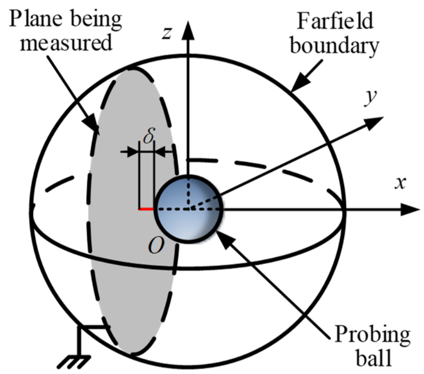

Figure 2. Model for analysis.

The electrical field analysis problem here can be taken as an electrostatic boundary value problem with a Dirichlet boundary condition, in which both the surface being measured and the far-field boundary are grounded, and the electrical potential of the probing ball is known. The electrical potential distribution U in the field can be expressed with Laplace's equation, as shown in Equation (1) below.

$$\nabla^2 U = 0, \tag{1}$$

Laplace's equation is expressed in a spherical coordinate as shown in Equation (2) in order to facilitate the calculation of the surface charge distribution on the probing ball.

$$\nabla^2 U = \frac{1}{r^2}\frac{\partial}{\partial r}\left(r^2\frac{\partial U}{\partial r}\right) + \frac{1}{r^2 \sin\theta}\frac{\partial}{\partial \theta}\left(\sin\theta\frac{\partial}{\partial \theta}\right) + \frac{1}{r^2 \sin^2\theta}\frac{\partial^2 U}{\partial \phi^2} = 0, \tag{2}$$

To solve Laplace's equation, a 3D seven-point finite difference scheme is proposed as shown in Equation (3), and the spatial relationship of the seven points is shown in Figure 3. This finite difference scheme is derived from the spherical coordinates with the origin located at the center of the probing ball. Thus, the electrical potential distribution U can be obtained with proper gridding and iteration.

$$U_0{}^{i+1} = \begin{cases} \left. \dfrac{r^2 \sin^2\theta h_1 h_2 h_3 h_4 h_5 h_6}{2r\sin^2\theta h_3 h_4 h_5 h_6 (r+h_2-h_1)+\sin^2\theta h_1 h_2 h_3 h_4 [2+(h_6-h_5)\cot\theta]+2h_1 h_2 h_5 h_6} \cdot \left[\begin{array}{l} \frac{2(r+h_2)}{rh_1(h_1+h_2)} U_1{}^i + \frac{2(r-h_1)}{rh_2(h_1+h_2)} U_2{}^i + \frac{2}{r^2\sin^2\theta h_3(h_3+h_4)} U_3{}^i \\ + \frac{2}{r^2\sin^2\theta h_4(h_3+h_4)} U_4{}^i + \frac{2+h_6\cot\theta}{r^2 h_5(h_5+h_6)} U_5{}^i + \frac{2-h_5\cot\theta}{r^2 h_6(h_5+h_6)} U_6{}^i \end{array} \right] \right|_{\theta\neq 0 \text{ and } \theta\neq\pi} \\ \left. \dfrac{h_4}{h_3+h_4} U_3{}^i + \dfrac{h_3}{h_3+h_4} U_4{}^i \right|_{\theta=0 \text{ or } \theta=\pi} \end{cases} \tag{3}$$

where $I = 1, 2, 3, \ldots$.

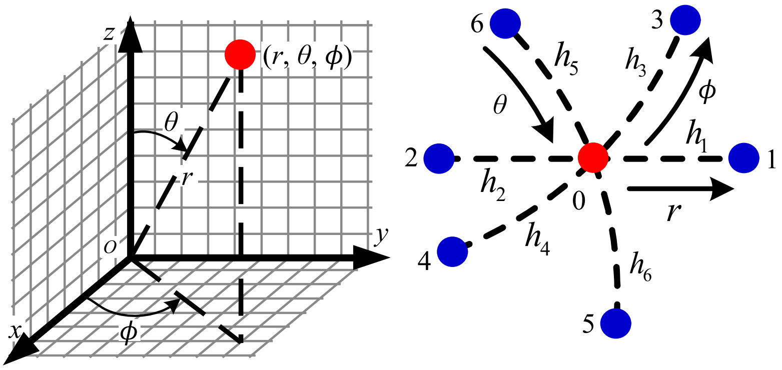

Figure 3. The spatial relationship of 7 points.

Considering the fact that the spherical scattering electrical field is extremely non-uniform, the grids in this method are generated non-uniformly from the spherical coordinates. As shown in Figure 4, fine grids are generated near the probing point while coarse grids are kept away from it. In addition, quick convergence is achieved by combining the over-relaxation iterative method and the non-uniform gridding in this study.

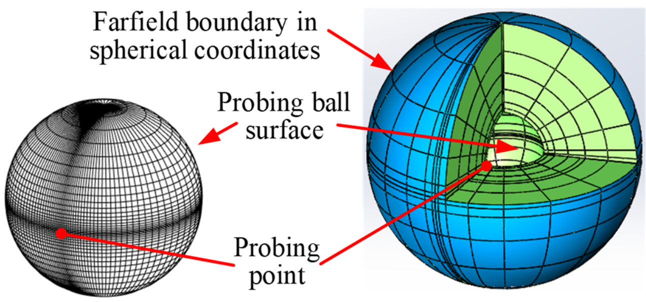

Figure 4. Schematic diagram of nonuniform gridding in spherical coordinates.

Electric field intensity distribution $\vec{E}$ can be obtained using Equation (4):

$$\vec{E} = -\nabla U \tag{4}$$

According to Gauss's law, charge density distribution σ on the surface of the probing ball can be expressed as Equation (5) since the probing ball is a conductive sphere,

$$\sigma = \varepsilon E, \tag{5}$$

where ε is the dielectric constant.

The distribution σ of the spherical surface charge on the probing ball can thus be obtained.

4. FEM Simulation Verification

In order to verify the effectiveness of the proposed method, FEM simulation is carried out by using COMSOL Multiphysics (COMSOL Inc, Burlington, MA, USA) to obtain the surface charge distribution σ over the spherical surface of the SSEP probing ball. The parameters used for the simulation are those commonly used in real situations. The diameter of the probing ball is ϕ1 mm, and the probing gap δ between the probing ball and the probed plane is 0.3 µm. The potential of the probing ball is set to be 1 V while the plane is grounded. The results for the surface charge distribution on the probing ball obtained with both methods are shown in Figure 5, in which the sphere stands for the probing ball of ϕ1 mm in diameter. An expanded view of surface charge distribution, in which the spherical surface is unfolded by polar angle θ and azimuthal angle ϕ, is shown in Figure 6 for clarity. The maximum relative differences in surface charge density on the probing point (θ = 90°, ϕ = 180°) of different probing balls between the modeling analysis and the simulation results are shown in Table 1, while the curves of the surface charge ratio as a function of the surface area ratio for different probing balls are shown in Figure 7. These curves are proposed to present the surface charge concentrating around the probing point, which is further discussed in Section 5.1. The surface charge ratio in this paper is referred to as the ratio between the surface charge on the area centering on the probing point and the total surface charge, while the surface area ratio is the ratio between the area centering on the probing point and the total surface area. It can be concluded that the results for the surface charge concentration obtained with the two methods perfectly match with each other, and the effectiveness of the method proposed can be verified through this comparison.

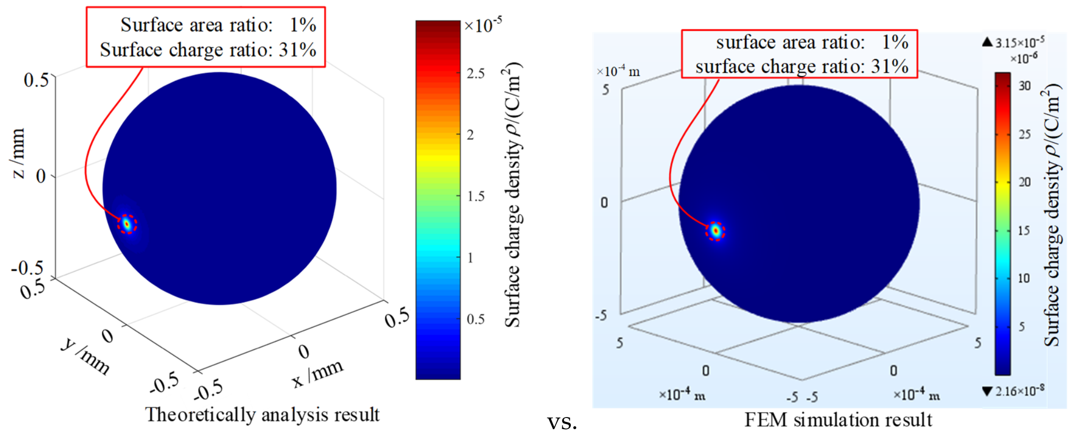

Figure 5. Modeling analysis and simulation results of surface charge distribution on the ϕ1 mm probing ball.

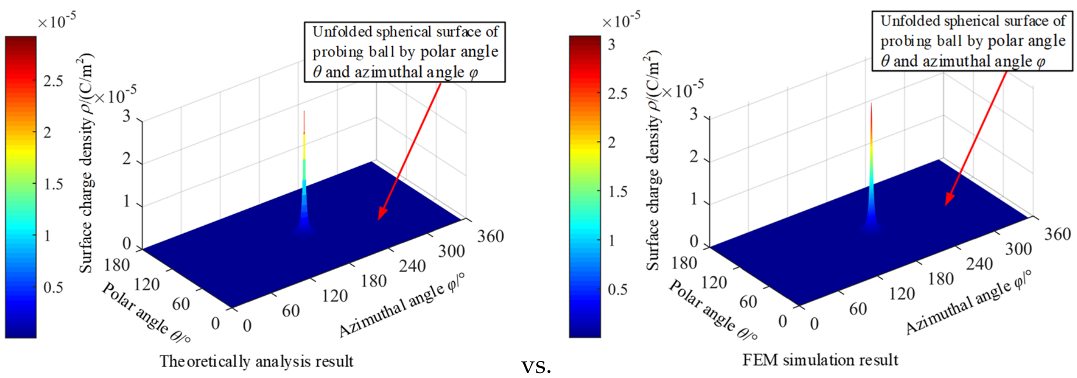

Figure 6. Modeling analysis and simulation results of surface charge distribution with the spherical surface unfolded.

Table 1. Maximum relative differences of surface charge density on the probing point of probing ball between modeling analysis and simulation results (δ = 0.3 µm).

Diameter of Probing Ball ϕ /mm	**0.1**	**0.5**	**1**	**2**
Maximum relative differences of surface charge density on probing ball	2.2%	5.9%	5.3%	4.2%

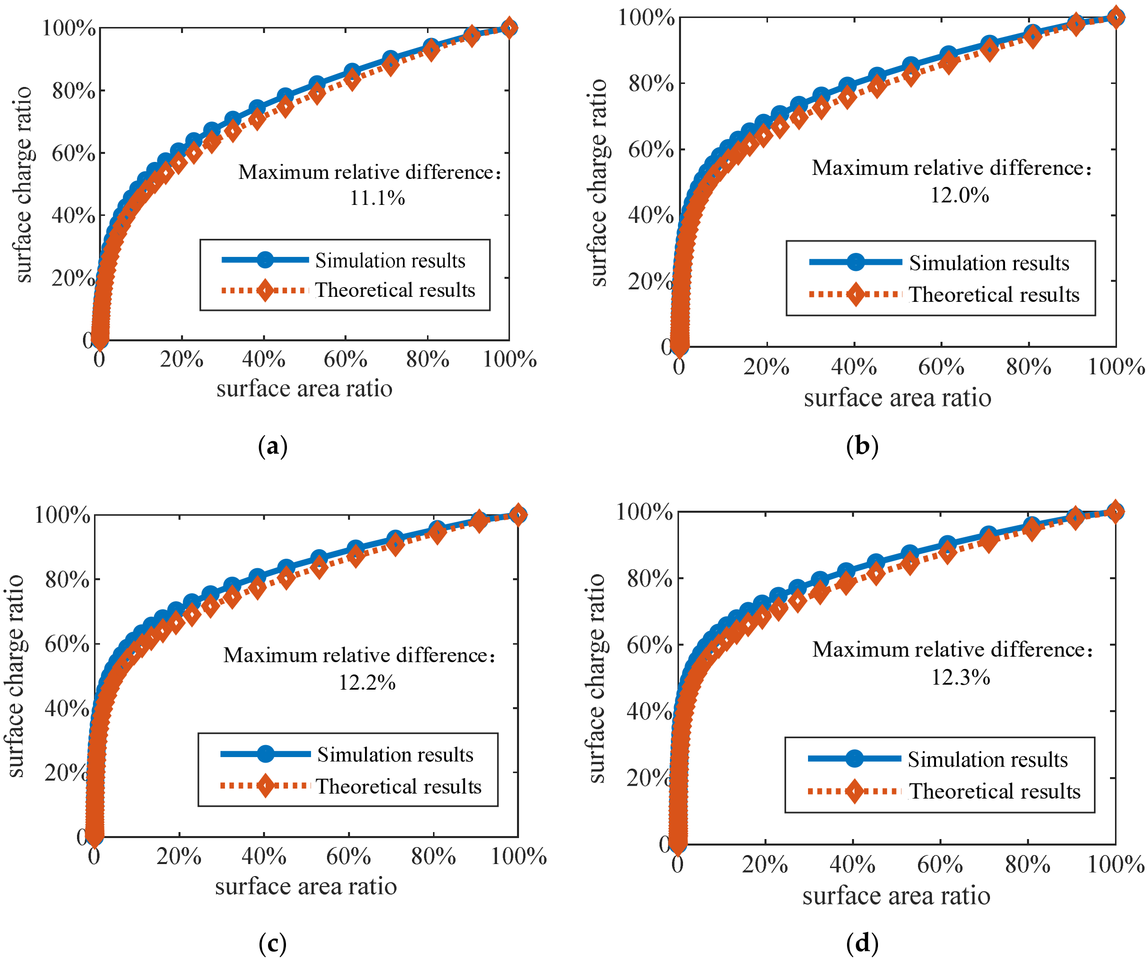

Figure 7. Surface charge ratio as a function of the surface area ratio for probing balls with different diameters. (**a**) ϕ0.1 mm; (**b**) ϕ0.5 mm; (**c**) ϕ1 mm; (**d**) ϕ2 mm.

5. Surface Charge Concentration Analysis

5.1. Surface Charge Concentration

To analyze the law of surface charge concentration, the surface charge density on the equatorial line (θ = 90°) of the probing ball is shown in Figure 8a, and the curve of the surface charge ratio as a function of the surface area ratio is shown in Figure 8b. For clarity, the small area centering on the probing point is referred to as the aiming area in this study. It can be seen that the surface charge density in the aiming area is much greater than that in other regions on the probing ball surface, with the diameter ϕ ranging from 0.1 mm to 2 mm. The analysis results in Figure 6 indicate that 31% of the total surface charge on the ϕ1 mm probing ball concentrates in the probing area, which accounts for 1% of the spherical surface area when a plane is probed by the gap of 0.3 µm.

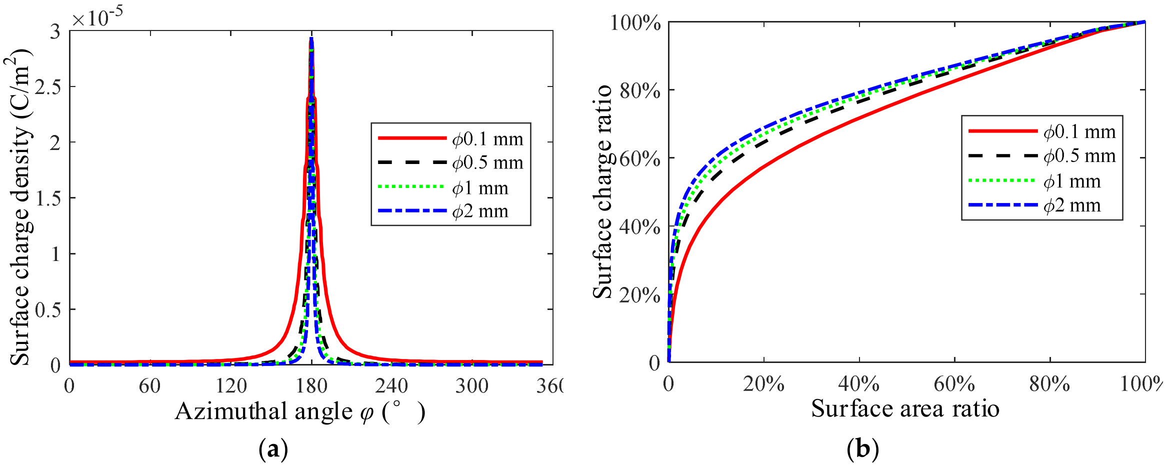

Figure 8. (**a**) Surface charge density on the equator of the probing ball; (**b**) surface charge ratio as a function of the surface area ratio.

5.2. Effect of the Probing Gap

The law of surface charge concentrations varying with probing gaps is shown in Figure 9 below. It can be seen that the relative charge amount on the aiming area increases as the probing gap decreases, and more than 42% of total surface charge stays in the small aiming area, which occupies only 1% of the total spherical surface area when the probing gap δ decreases to 0.01 µm, while the trend of surface charge concentration remains the same for different probing gaps.

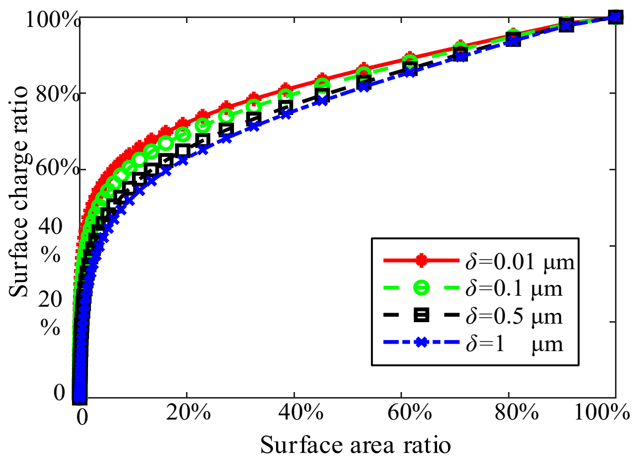

Figure 9. Surface charge ratio as a function of surface area ratio for different probing gaps.

5.3. Effect of Surface Geometry

In addition, to analyze the pattern of surface charge changes with the shape of the surface being measured, surface charge distributions on the probing ball are analyzed when the SSEP is used to probe the interior surfaces of cylindrical surfaces of ϕ6 mm and ϕ12 mm in diameter, and spherical surfaces of ϕ6 mm and ϕ12 mm in diameter. Other conditions are the same as the previous analyses, with ϕ1 mm probing ball and 0.3 µm probing gap δ. It can be seen from Figure 10 that the surface charge concentrations of the SSEP are all well in line when cylindrical surfaces, spherical surfaces, and planes are probed.

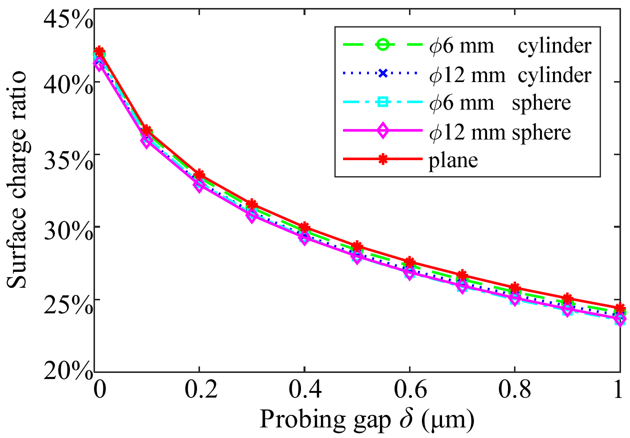

Figure 10. Surface charge ratio as a function of probing gaps on surfaces of different geometries (surface area ratio = 1%).

From the presentation in Figures 9 and 10, surface charge concentration on the probing ball is not only obvious but also similar when either the plane, the cylindrical surface, or the spherical surface is probed, and this concentration basically remains unchanged for different probing gaps in the sensing range. For common miniature internal structures with high aspect ratios, plane, cylindrical surface, and spherical surface are the main composition elements. It can therefore be concluded that the SSEP is of surface charge concentration characteristics when probing miniature internal structures of various free geometrical shapes.

5.4. Point Probing Characteristics

The variation of surface charge on the probing ball of the SSEP can be transformed into the variation of probing gap and even further displacement signal through detection of the charge signal. Similar to high surface charge density near the probing point, the electrical field intensity near the probing point is much stronger than that in any other region. Therefore the probing point and the tiny area centering on it have the strongest effect on the probing characteristics of the SSEP, and this unique characteristic proves the approximate point probing capacity of the SSEP. A virtual "needle" of electrical effect is formed, and thus the SSEP can pick up high-frequency spatial information. Together with its non-contact and 3D isotropy capability as well as nanometer resolution, the SSEP simultaneously possesses all the essentials for high-precision measurement of miniature structures with high aspect ratios, which no other single conventional measurement method possesses simultaneously.

As shown in Figure 11, the lack of measurement methods for internal structures with aspect ratios over 10:1, for which SEM is not suitable to be applied, could be filled with methods based on SSEP.

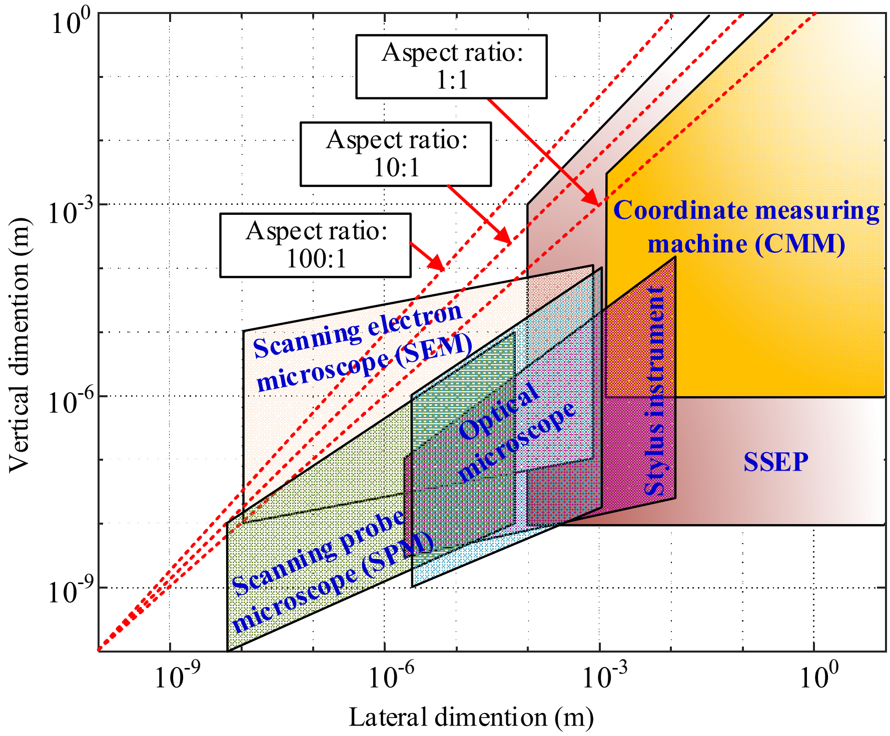

Figure 11. Measurement methods for dimensional micro- and nanometrology (inspired by Ref. [28], in this figure the "CMM" refers to a coordinate measuring machine (CMM) with traditional probes, and "SSEP" refers to SSEP used with CMM).

6. Conclusions

The spherical scattering electrical field of the SSEP formed during probing was modeled by a 3D seven-point finite difference method, and the characteristics and law of surface charge distribution on the probing ball of the SSEP were analyzed and verified with FEM simulation. Analysis results indicate that the surface charge on the probing ball of SSEP has the characteristic of concentrating towards the probing point. When a probing ball of ϕ1 mm in diameter probes a grounded plane with a microprobing gap of 0.3 µm, more than 31% of surface charge on the probing ball concentrates in the aiming area, which covers 1% of the total probing ball surface. The surface charge concentration remains the same when surfaces of different geometrical shapes are probed with different probing gaps in the sensing range, demonstrating the approximate point sensing capacity of the SSEP. Together with its non-contact and 3D isotropy sensing capability as well as nanometer resolution, the SSEP has all the necessary characteristics required for precision measurement of miniature internal structures with high aspect ratios, showing great potential to remedy the lack of measurement methods for internal structures with aspect ratios over 10:1. Our future work will focus on miniaturization of the SSEP.

Author Contributions: Conceptualization, J.C. and X.B.; Funding acquisition, J.C.; Methodology, X.B. and J.C.; Project administration, J.C. and J.T.; Software, X.B. and Y.L.; Validation, Y.Z. and Z.C.; Writing—original draft, X.B. All authors have read and agreed to the published version of the manuscript.

Funding: This research was funded by the National Natural Science Foundation of China, grant number 51675139, L1924059 and the Fundamental Research Funds for The Central Universities.

Conflicts of Interest: The authors declare no conflict of interest.

References

1. Tan, J.B.; Cui, J.N. Ultraprecision 3d probing system based on spherical capacitive plate. *Sens. Actuator A Phys.* **2010**, *159*, 1–6. [CrossRef]

2. Bian, X.; Cui, J.; Lu, Y.; Tan, J. Ultraprecision diameter measurement of small holes with large depth-to-diameter ratios based on spherical scattering electrical-field probing. *Appl. Sci.* **2019**, *9*, 242. [CrossRef]
3. Bos, E.J.C. Aspects of tactile probing on the micro scale. *Precis. Eng. J. Int. Soc. Precis. Eng. Nanotechnol.* **2011**, *35*, 228–240. [CrossRef]
4. Bauza, M.B.; Woody, S.C.; Woody, B.A.; Smith, S.T. Surface profilometry of high aspect ratio features. *Wear* **2011**, *271*, 519–522. [CrossRef]
5. Hansen, H.N.; Carneiro, K.; Haitjema, H.; De Chiffre, L. Dimensional micro and nano metrology. *CIRP Ann. Manuf. Technol.* **2006**, *55*, 721–743. [CrossRef]
6. Neugebauer, M.; Lüdicke, F.; Bastam, D.; Bosse, H.; Reimann, H.; Töpperwien, C. A new comparator for measurement of diameter and form of cylinders, spheres and cubes under clean-room conditions. *Meas. Sci. Technol.* **1997**, *8*, 849–856. [CrossRef]
7. Thalmann, R. A New High Precision Length Measuring Machine. In Proceedings of the 8th International Metrology Congress, Besançon, France, 20–23 October 1997; pp. 1–4.
8. Weckenmann, A.; Estler, T.; Peggs, G.; McMurtry, D. Probing systems in dimensional metrology. *CIRP Ann. Manuf. Technol.* **2004**, *53*, 657–684. [CrossRef]
9. Zhao, Y.; Li, P.; Wang, C.; Pu, Z. A novel fiber-optic sensor used for small internal curved surface measurement. *Sens. Actuator A Phys.* **2000**, *86*, 211–215. [CrossRef]
10. Weiqian, Z.; Jiubin, T.; Lirong, Q.; Limin, Z. A new laser heterodyne confocal probe for ultraprecision measurement of discontinuous contours. *Meas. Sci. Technol.* **2005**, *16*, 497.
11. Schmitt, R.; Mallmann, G. Evaluation of the usage of a fiber optic low-coherence interferometer for surface profile measurements using speckles analysis. In Proceedings of the Speckle 2010: Optical Metrology, Florianapolis, Brazil, 13–15 September 2010; p. 73870N.
12. Depiereux, F.; Konig, N.; Pfeifer, T.; Schmitt, R. Fiber-based white-light interferometer with improved sensor tip and stepped mirror. *IEEE Trans. Instrum. Meas.* **2007**, *56*, 2279–2283. [CrossRef]
13. Cui, J.; Li, L.; Li, J.; Tan, J.B. Fiber probe for micro-hole measurement based on detection of returning light energy. *Sens. Actuator A Phys.* **2013**, *190*, 13–18. [CrossRef]
14. Shiramatsu, T.; Kitano, K.; Kawada, M.; Mitsui, K. Development of measurement method for shape and dimension of micro-components. *JSME Int. J. Ser. C* **2004**, *47*, 369–376. [CrossRef]
15. McMurtry, D. The development of sensors for cmms. *Laser Metrol. Mach. Perform. VI* **2003**, *44*, 205–220.
16. Oiwa, T.; Nishitani, H. Three-dimensional touch probe using three fibre optic displacement sensors. *Meas. Sci. Technol.* **2004**, *15*, 84. [CrossRef]
17. Takamasu, K.; Chih-Che, K.; Suzuki, A.; Hiraki, M.; Furutani, R.; Ozono, S. Development of pneumatic ball probe for measuring small hole. In Proceedings of the International Conference on Precision Engineerin, Taipei, Taiwan, 20–22 November 1997.
18. Bowers, W.J.; Olson, D.A. A capacitive probe for measuring the clearance between the piston and the cylinder of a gas piston gauge. *Rev. Sci. Instrum.* **2010**, *81*, 035102. [CrossRef] [PubMed]
19. Dai, G.; Heidelmann, M.; Kübel, C.; Prang, R.; Fluegge, J.; Bosse, H. Reference nano-dimensional metrology by scanning transmission electron microscopy. *Meas. Sci. Technol.* **2013**, *24*, 085001. [CrossRef]
20. Peiner, E.; Doering, L. Nondestructive evaluation of diesel spray holes using piezoresistive sensors. *IEEE Sens. J.* **2013**, *13*, 701–708. [CrossRef]
21. Kang, H.; Lim, M.; Yun, K. Characterization of the electric field concentration between two adjacent spherical perfect conductors. *SIAM J. Appl. Math.* **2014**, *74*, 125–146. [CrossRef]
22. Morales, M.; Diaz, R.A.; Herrera, W.J. Solutions of laplace's equation with simple boundary conditions, and their applications for capacitors with multiple symmetries. *J. Electrost.* **2015**, *78*, 31–45. [CrossRef]
23. Johann, F.; Soergel, E. Quantitative measurement of the surface charge density. *Appl. Phys. Lett.* **2009**, *95*, 232906. [CrossRef]
24. Villeneuve-Faure, C.; Boudou, L.; Makasheva, K.; Teyssedre, G. Methodology for extraction of space charge density profiles at nanoscale from kelvin probe force microscopy measurements. *Nanotechnology* **2017**, *28*, 505701. [CrossRef] [PubMed]
25. Kumada, A.; Shimizu, Y.; Chiba, M.; Hidaka, K. Pockels surface potential probe and surface charge density measurement. *J. Electrost.* **2003**, *58*, 45–58. [CrossRef]
26. Deng, J.; Kumada, A.; Hidaka, K.; Zhang, G.; Mu, H. Residual charge density distribution measurement of surface leader with feedback electrostatic probe. *Appl. Phys. Lett.* **2012**, *100*, 192906. [CrossRef]

27. Okamoto, T.; Kitagawa, S.; Inoue, N.; Ando, A. Electric field concentration in the vicinity of the interface between anode and degraded BaTiO3-based ceramics in multilayer ceramic capacitor. *Appl. Phys. Lett.* **2011**, *98*, 072905. [CrossRef]
28. De Chiffre, L.; Kunzmann, H.; Peggs, G.N.; Lucca, D.A. Surfaces in precision engineering, microengineering and nanotechnology. *CIRP Ann.* **2003**, *52*, 561–577. [CrossRef]